AGU ADVANCING EARTH AND SPACE SCIENCES

Geophysical Research Letters

RESEARCH LETTER
10.1029/2025GL116554

Revisiting the Diurnal Pulses of Tropical Cyclones Over the Northwest Pacific Ocean

Jinjing Zhang[1,2,3] and **Yu Du**[1,2,3]

[1]School of Atmospheric Sciences, Sun Yat-sen University, and Southern Marine Science and Engineering Guangdong Laboratory (Zhuhai), Zhuhai, China, [2]Guangdong Province Key Laboratory for Climate Change and Natural Disaster Studies, Sun Yat-sen University, Zhuhai, China, [3]Key Laboratory of Tropical Atmosphere-Ocean System, Ministry of Education, Sun Yat-sen University, Zhuhai, China

Key Points:

- The discontinuity in diurnal pulses (DPs) results from the combination of an outward-propagating mode and quasi-phase-locked modes
- DPs are likely driven by inertial-gravity waves in 0–30°N latitude, and by tropical cyclone (TC) outflow wind advection north of 30°N
- DPs of TCs share similar characteristics and mechanisms with the offshore propagation of coastal rainfall

Supporting Information:

Supporting Information may be found in the online version of this article.

Correspondence to:

Y. Du,
duyu7@mail.sysu.edu.cn

Citation:

Zhang, J., & Du, Y. (2025). Revisiting the diurnal pulses of tropical cyclones over the Northwest Pacific ocean. *Geophysical Research Letters*, *52*, e2025GL116554. https://doi.org/10.1029/2025GL116554

Received 16 APR 2025
Accepted 28 JUN 2025

Abstract This study investigates the characteristics and mechanisms of diurnal pulses (DPs) in tropical cyclones (TCs) over the Northwest Pacific. Previous studies have noted discontinuities in DP propagation with respect to radius, but lacked an explanation for this phenomenon. Our findings reveal that this discontinuity results from the superposition of an outward-propagating mode driven by inertial-gravity waves and quasi-phase-locked signals associated with the diurnal variations in the TC secondary circulation. DP occurrence exhibits strong latitude dependence. DPs occur more frequently within 0°–30°N latitude, likely driven by inertial-gravity waves originating from the TC inner core at the tropopause. North of 30°N, DP propagation is primarily influenced by the TC outflow winds, with the DP propagation speed strongly correlated to outflow strength. Additionally, DPs share similarities in characteristics and mechanisms with the offshore propagation of coastal rainfall, both governed by inertial-gravity waves in lower latitudes and by wind advection at higher latitudes.

Plain Language Summary Diurnal pulses (DPs) are outward-propagating cold cloud features at high altitudes found in tropical cyclones (TCs). Previous studies have observed an apparent break in DP propagation, where DP composite pattern shows "two-segment" propagation in the inner and outer regions of the TC. Our study explains that although DPs move continuously outward, they are superimposed with quasi-phase-locked diurnal signals associated with the TC secondary circulation, creating the appearance of a discontinuity. We propose that analyzing DP anomalies can help separate the true continuous DP signal from the combination of these two behaviors. In addition, DPs in TCs share similarities with offshore propagation of coastal rainfall. Both occur more frequently within 0°–30°N latitude, mainly influenced by inertial-gravity waves, while at higher latitudes, their movements are largely dependent on TC outflow or background winds.

1. Introduction

Diurnal variations in radiation play a crucial role in the development of convection systems over the ocean. Nighttime cooling enhances nocturnal instability (Kraus, 1963; Randall et al., 1991) and relative humidity (Dudhia, 1989; Tao et al., 1996). The differential nighttime cooling between cloud-covered and cloud-free regions strengthens low-level convergence (Gray & Jacobson, 1977). These mechanisms contribute to nighttime intensification and the pronounced diurnal cycles in clouds, rainfall and convective structures (Ruppert & Hohenegger, 2018; Ruppert & Johnson, 2016).

Tropical cyclones (TCs), as organized mesoscale convective systems over the ocean, also display significant diurnal variations in intensity, structure, and convection (Bowman & Fowler, 2015; Hong & Wu, 2023; Leppert & Cecil, 2016; Ruppert & O'Neill, 2019; Tang & Zhang, 2016; Wu & Ruan, 2016; Wu et al., 2015; X. Zhang & Xu, 2024). The extensive TC cirrus canopy plays a critical role in radiative and convective diurnal changes. At night, enhanced cloud top longwave cooling promotes the inner-core deep convection and the lower-to-mid-level circulation, accompanied by observed increases in boundary layer inflow within the TC (J. A. Zhang et al., 2020). During the day, shortwave radiation suppresses deep convection, promotes upper-level circulation and enhances TC outflow (Navarro et al., 2017; Ruppert & O'Neill, 2019).

A prominent feature of the TC diurnal cycle is the cooling signal of upper-level cold clouds, characterized by low brightness temperatures (BT), which propagate radially outward from the TC center and are referred to Diurnal Pulses (DPs) (Ditchek, Molinari, et al., 2019; Dunion et al., 2014; Piersante et al., 2023; X. Zhang et al., 2023).

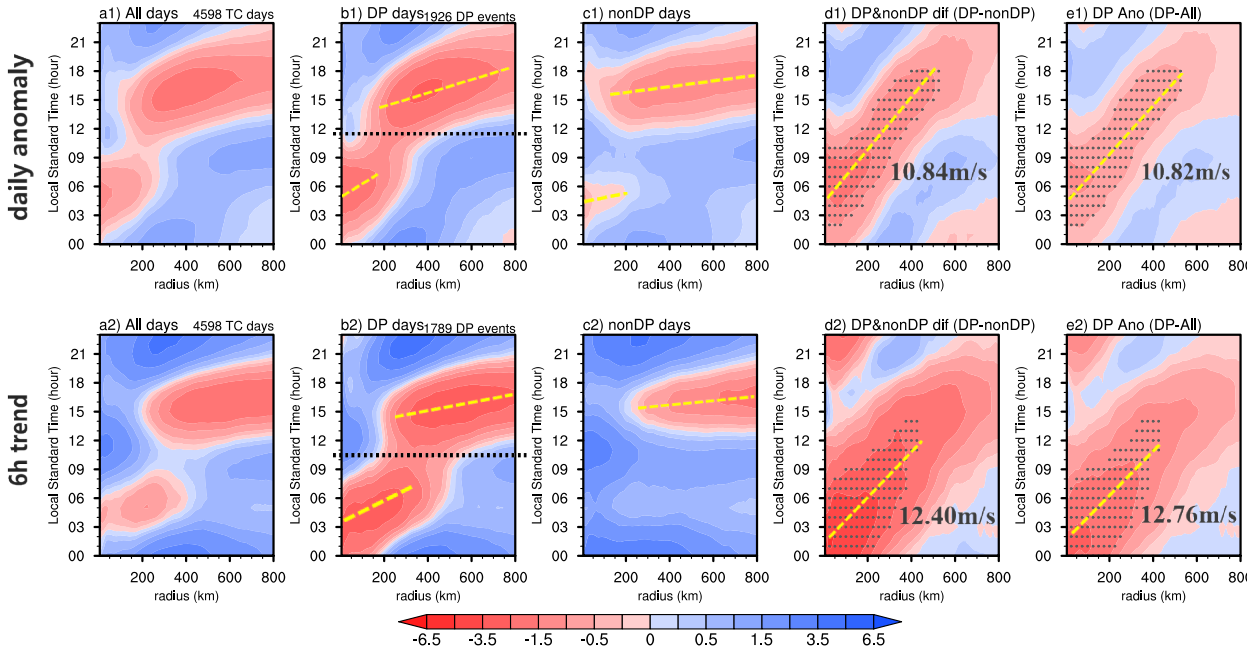

Figure 1. The composite Hovmöller diagrams of azimuthally averaged brightness temperatures (a1–e1) daily anomalies (K) and (a2–e2) 6-hr trends (K) for (a1, a2) all tropical cyclone (TC) days, (b1, b2) diurnal pulse (DP) days, (c1, c2) non-DP days, (d1, d2) the difference between DP days and non-DP days, and (e1, e2) the difference between DP days and all TC days (DP anomaly). Dots indicate grids used for speed calculation, with a 20th percentile threshold for each subplot. Speeds are derived from the temporal medians of grid points corresponding to each radius via linear regression.

DPs typically form in the inner core near sunset and propagate several hundred kilometers outward by the following afternoon (Dunion et al., 2014), occurring on 52% of TC days globally (X. Zhang et al., 2023). Although there is quasi-continuous propagation within individual DP events, composite DP signals show a discontinuity between the inner and outer regions with two-segment propagations (Fig. 8 in X. Zhang et al. (2023) and Figure 1). This discontinuity is characterized by a distinct weakening and deceleration of the pulse between 09:00 and 12:00 local standard time (LST) within 200–400 km radius, followed by reacceleration and intensification beyond 400 km after 15:00 LST—a phenomenon that remains unexplained.

Previous studies have documented that DPs are closely related to changes in TC structure and intensity, with evidence of coupling between DP, precipitation, and deep convective structure (Ditchek et al., 2020; Ditchek, Corbosiero, et al., 2019; Ditchek, Molinari, et al., 2019; Trabing & Bell, 2021; X. Zhang & Xu, 2022, 2024). DPs are also considered a significant precursor to TC rapid intensification (X. Zhang & Xu, 2021). Outward-propagating signals in convection have been detected in deep layer alongside DPs (Dunion et al., 2014), and a squall-line-like feature in vertical velocity has been observed throughout the TC environment (Ditchek et al., 2020; Dunion et al., 2019). These findings suggest that DPs might not be confined to the outflow layer, but instead correspond to coupled oscillations extending through the deep layer of the TC environment.

Given the significant influence of diurnal variations in radiative and convective heating on TCs, previous studies suggest that DPs are associated with diurnal inertial-gravity waves, with an average propagating speed of 11–13 m s^{-1}, similar to the phase speed of these waves (Ditchek, Corbosiero, et al., 2019; X. Zhang et al., 2023). Similar to clouds and precipitation, numerical models show spatially coherent diurnal changes in temperature and radial wind, both horizontally and vertically, consistent with gravity waves characterized by horizontal wavelengths of approximately 1,000 km. These waves are triggered by diurnal forcing at the height of TC outflow layer (13–14 km) (Navarro & Hakim, 2016; O'Neill et al., 2017). However, while the inertial-gravity-wave mechanisms of DPs have primarily explored through numerical simulations, the evidence provided by statistical analyses calls for further investigation.

Similarly, near global coastlines, land-sea breeze circulations can excite inertial-gravity waves in response to land-sea thermal contrast (Du & Rotunno, 2015; Jiang, 2012; Rotunno, 1983), resulting in the nighttime offshore propagation (OP) of coastal precipitation (Du & Rotunno, 2018; Kilpatrick et al., 2017; Li & Carbone, 2015). OP

occurs along 78% of global coastlines at an average speed of approximately 13 m s^{-1}, with a strong latitude dependence: within 0°–30° latitude, OP is primarily controlled by inertial-gravity waves, whereas poleward of 30°, offshore background winds play a dominant role (Fang & Du, 2022). OP shares conceptual similarities with the DPs in TCs in both propagating speeds and its association with inertial-gravity waves, suggesting a possible connection between the two phenomena.

The Northwest Pacific (WNP) is the most active TC genesis basin worldwide, and TCs in this region exhibit the highest occurrence rate of DPs among all ocean basins (X. Zhang et al., 2023). This study revisits DPs of TCs over the WNP and seeks to address three key scientific questions to deepen our understanding of DP characteristics and the dynamic mechanisms driving TC diurnal variations:

1. What causes the discontinuity in composite DP signal between the inner and outer regions?
2. Do DPs exhibit a latitude-dependent inertial-gravity wave mechanism based on observed statistics?
3. What is the relationship between DPs in TCs and OP near the coast?

2. Data and Methods

2.1. Data

Three-hourly TC track data from 2001 to 2022 are obtained from the International Best Track Archive for Climate Stewardship (IBTrACS) version 4 (Kenneth et al., 2019; Knapp et al., 2010) to acquire time series and central coordinates for each TC. Cloud top infrared BT with a three-hour temporal resolution and a spatial resolution of 0.07° are obtained from NOAA's Gridded Satellite (GridSat) B1 data set (Knapp et al., 2011) to characterize TC cold clouds and identify DP events.

Atmospheric variables are derived from the hourly fifth-generation global atmospheric reanalysis data sets (ERA5) produced by ECMWF. ERA5 data have a horizontal resolution of 0.25° and include 37 vertical levels from 1,000 to 1 hPa (Copernicus Climate Change Service, 2018). ERA5 data are used to diagnose TC outflow, cloud, secondary circulation and gravity-wave features, as well as to calculate radiative heating rate. Previous studies have confirmed that ERA5 offers reliable and validated data sets for examining diurnal-scale gravity waves, particularly in large-scale statistical analyses (Chen & Du, 2024; Chen et al., 2025; Du, 2023). To ensure temporal consistency, only ERA5 data corresponding to IBTrACS timestamps are used for calculations. All data are linearly interpolated to hourly LST and regridded onto a TC-center polar coordinate system: BTs data are mapped with 5-km radial spacing (0–800 km) and 2-degree azimuthal intervals, while ERA5 data adopt 20-km radial spacing and 6-degree azimuthal intervals.

2.2. Definition and Identification of DP Signals

Following the approach outlined by X. Zhang et al. (2023), we identify DP events for 543 WNP TCs from 2001 to 2022 using two methods: (a) daily BT anomaly, calculated as the difference from a 24-hr moving average, and (b) 6-hr BT trend difference, determined as the current BT minus the BT from 6 hr prior. Significant cooling grid points are identified through azimuthally averaged Hovmöller diagrams at 20-km radial and 3-hourly temporal resolutions, For each method, significant cooling is identified using the 25th percentile thresholds: −3.02 K for the daily anomaly method and −3.96 K for 6-hr trend method.

A DP event is defined as a continuous propagation of significant cooling grid points that meets the criteria set by X. Zhang et al. (2023), including a minimum duration of 6 hr, a propagation length of at least 300 km, and the selection of the largest cluster per day. Based on these criteria, we identify a total of 1926 DP events from 4598 TC days using the daily anomaly method, and 1789 DP events using 6-hr trend method. In addition, TC days containing DP events are classified as DP days, while those without are categorized as non-DP days.

3. Results

3.1. Characteristics of DP Occurrence

3.1.1. DP Under Different Definitions

To analyze the characteristics of DP occurrence, we compose cloud top infrared BTs for all TC days, DP days, and non-DP days using both the daily anomaly and 6-hr trend methods (Figure 1).

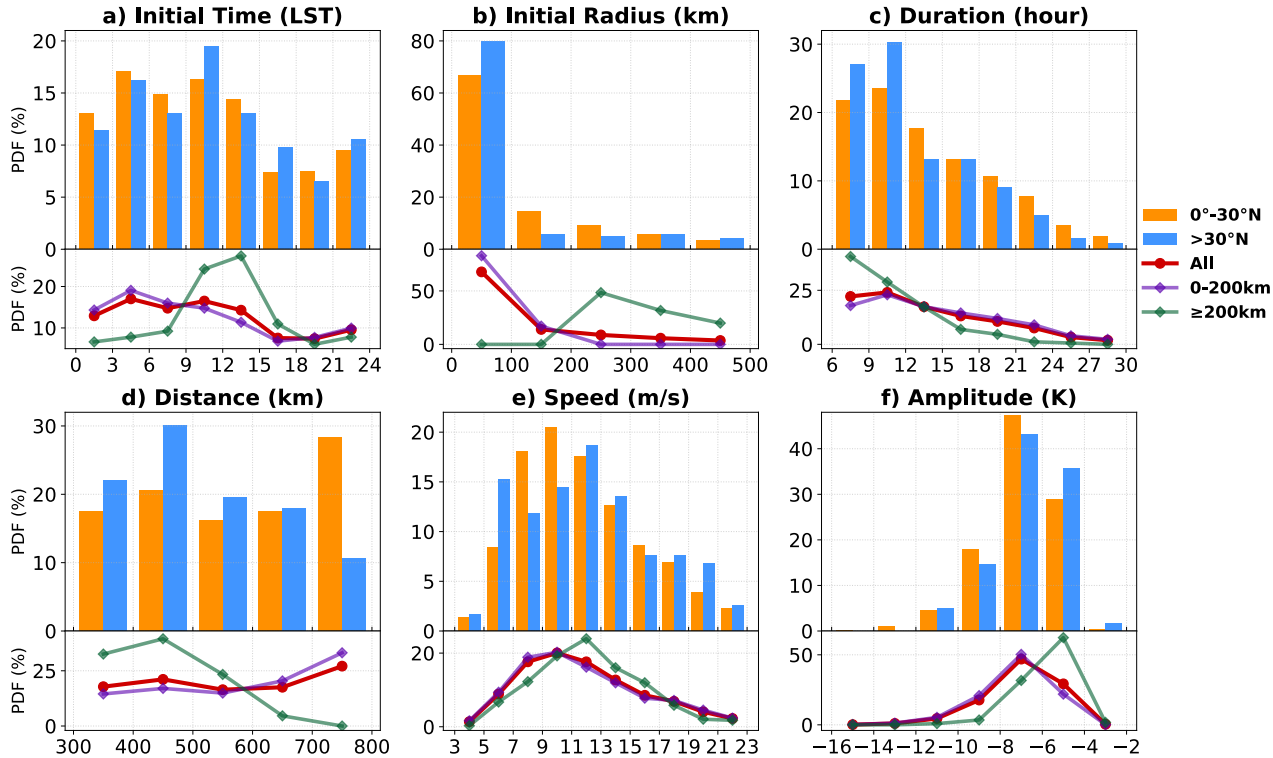

Figure 2. Probability distribution function of diurnal pulse events characteristics, categorized by (a) initial time (LST), (b) initial radius (km), (c) duration (hr), (d) propagating distance (km), (e) propagating speed (m s^{-1}), and (f) pulse amplitude (K). Red lines represent all events; purple and green lines correspond to events initiating within 0–200 km and beyond 200 km radius, respectively. Orange and blue bars indicate events occurring within 0°–30°N and north of 30°N, respectively.

The composite BT patterns obtained from the two methods are largely consistent, but the 6-hr trend method identifies DP initiation approximately 3 hr earlier. While the daily anomaly method yields slightly weaker amplitude signals, both methods exhibit comparable propagation speeds. On DP days (Figures 1b1 and 1b2), both methods display two distinct outward-propagating cooling signals, consistent with X. Zhang et al. (2023). The first signal occurs within 0–200 km from night to early morning, while the second develops within 200–800 km from afternoon to evening, with the latter propagating at a faster rate.

The discrepancies observed in initial time and amplitude between the daily anomaly and 6-hr trend methods arise from differences in calculation. A variable exhibiting diurnal variation can be represented as $f(t) = A\sin\left(t \times \frac{\pi}{24} + \varphi\right) + C$, where t is the LST (hour), A is the amplitude, φ is the initial phase, C is constant, and the 24-hr period reflects the diurnal cycle. In the daily anomaly method, the diurnal signal is extracted by subtracting the diurnal mean (C) from $f(t)$, yielding $f_1(t) = A\sin\left(t \times \frac{\pi}{24} + \varphi\right)$. In contrast, the 6-hr trend method approximates the diurnal variation by differencing values separated by 6 hr: $f_2(t) = A\sin\left(t \times \frac{\pi}{24} + \varphi\right) - A\sin\left[(t-6) \times \frac{\pi}{24} + \varphi\right] = \sqrt{2}A\sin\left(t \times \frac{\pi}{24} + \varphi + \frac{\pi}{4}\right) = \sqrt{2}A\sin\left[.(t+3) \times \frac{\pi}{24} + \varphi\right]$. This indicates that the trend method amplifies the diurnal signals by a factor of $\sqrt{2}$ and introduces a π/4 phase lead, equivalent to a 3-hr advance in time. Despite these differences, both methods yield consistent initial location, duration, propagating distance, and propagating speed. However, DPs identified using the daily anomaly method peak later and exhibit weaker amplitudes (Figures 2a and 2f) compared to X. Zhang et al. (2023) that used the trend method, highlighting the sensitivity of the diurnal phase to the chosen definition method. While the daily anomaly method better preserves the natural diurnal cycle, the trend method enhances signal strength but introduces a phase shift. Since the daily anomaly approach more accurately represents the natural diurnal phase compared to the trend method, it is used for the subsequent analysis in this study.

Another interesting observation is that a portion of DP events exhibit an "off-the-clock" behavior (Figure 2a), initiating at different LST from the "diurnal clock" described by Dunion et al. (2014). The second most common initial time for all DPs, especially for DPs within 0°–30°N, occurring between 9 and 15 LST, is mainly attributed

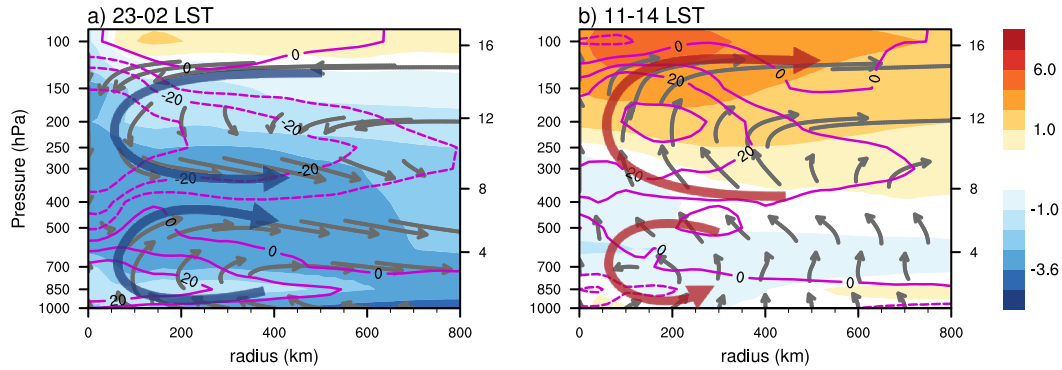

Figure 3. Azimuthally averaged cross-sections of radiative heating rate (shaded, K day^{-1}), diurnal anomalies in secondary circulation (vectors) and specific cloud ice + liquid content (contour, mg kg^{-1}) on non-DP days: (a) nighttime (23–02 LST) and (b) daytime (11–14 LST). Bold arrows indicate the relative two-layered circulation structure.

to events initiating from the outer region beyond a 200-km radius. This latter initial time may reflect signals which are indiscernible in the inner-core but become detectable in the outer region. In contrast, DPs initiating from the inner-core (0–200-km radius) occur most frequently at night, consistent with the "diurnal clock," with a smaller fraction of "off-the-clock."

3.1.2. Decomposition of the DP Signal

While individual DP events propagate continuously outward from the core of TC, the composite DP signal exhibits a discontinuous propagation pattern characterized by a distinct "two-segment" feature (Figure 1b1), which has not been fully explained in previous studies. However, our analysis reveals that DP anomaly, the difference signal between DP and non-DP days or all days (Figures 1d and 1e), exhibits continuous outward propagation. These composite DP anomalies initiate in the early morning from the inner core and travel at approximately 10 m s^{-1}, reflecting the diurnal-wave nature of DPs. Additionally, similar propagation behavior is observed in the upper-level ice condensate (figure not shown), indicating the correlation between BT cooling and condensate growth. Unlike DP composites, the propagating mode can be isolated by analyzing DP anomalies.

Interestingly, BT on non-DP days shows two quasi-phase-locked signals: one from the inner core (0–200 km during 03–06 LST) and another from the outer-region component (200–800 km during 13–20 LST) (Figure 1c1). The outer-region component extends to approximately 1,200 km radius (figure not shown), likely corresponding to the typical outer boundary of the TC secondary circulation. Therefore, the composite DP-day signal results from the combination of an outward-propagating mode and two inherent phase-locked modes, which naturally explains the observed discontinuous propagation and the "two-segment signal," where weakening occurs between 09 and 12 LST. This finding suggests the observed discontinuity is not caused by distinct propagation mechanisms between inner and outer regions, but rather is a result of the interaction between these multiple modes.

The quasi-phase-locked signals are driven by diurnal variations in the TC's secondary circulation. Figure 3 displays the radiative heating rate Q_R and diurnal anomalies in vertical-radial flow during both nighttime and daytime on non-DP days. Q_R (K day^{-1}) is calculated from the Lagrangian derivative of moist static energy $h = c_pT + Lq + gz$ (J kg^{-1}) with tangential average as derived by Ruppert and Hohenegger (2018):

$$\frac{Dh}{Dt} = \frac{\left(c_p + \frac{Lq}{T}\right) Q_R}{86400}, \tag{1}$$

where $c_p = 1005$ J kg^{-1} K^{-1} is the specific heat of dry air at constant pressure, $L = 2.54 \times 10^6 - 2910 \times (T - 273)$ J kg^{-1} is the heat of condensation, where T (K) is the temperature. During the nighttime on non-DP days, surface convergence enhances upward motion at mid-to-lower levels (Figure 3a), promoting stronger deep convection. The deep convective clouds undergo longwave cooling in the inner-core cloud top, which is reflected in the cooling BT observed within 200 km at night (Figure 1c1).

Conversely, during the daytime on non-DP days, shortwave radiation heats the upper-level clouds and promotes the mid-to-upper-level secondary circulation (Figure 3b). This leads to an overall lifting of the cirrus canopy and an increase in condensate due to adiabatic cooling. The increased cloud top height and enhanced ice crystal content contribute to the quasi-phase-locked BT cooling observed in the afternoon over the TC's outer-region (Figure 1c1).

Therefore, this finding offers the first statistical explanation for the observed DP discontinuity supported by observational evidence, improving upon previous studies that lacked such decomposition.

3.2. Latitude Dependence of DP

The DP continuous propagation mode has been hypothesized to be linked to inertial-gravity waves. Based on wave theory, the dispersion relation for the hydrostatic inertial-gravity waves in a rotating, stably stratified atmosphere (Navarro & Hakim, 2016; O'Neill et al., 2017) is:

$$\omega^2 = f^2 + \frac{N^2 k^2}{m^2}, \tag{2}$$

where ω is the diurnal frequency, f is the Coriolis frequency at a specific latitude, N is the Brunt–Väisälä frequency, k is the radial wavenumber and m is the vertical wavenumber. Note that Equation 2 neglects the inertial component associated with relative vorticity, which is a reasonable approximation in a TC environment, except the very near-core region (Navarro & Hakim, 2016; O'Neill et al., 2017). Given $\omega^2 - f^2 = \frac{N^2k^2}{m^2} > 0$, the inertial-gravity waves only survive within latitudes of 0°–30°.

If diurnal inertial-gravity waves play a key role in DP behavior, DPs should exhibit strong latitude dependence. Our statistics show that DPs occur on 49.1% of TC days within 0°–30°N, which is significantly higher than the 11.0% occurrence north of 30°N. Within 0°–30°N, DP anomalies display clear outward propagation with continuous phase and speed, along with a farther-reaching distance (Figure 4a). In contrast, north of 30°N, DP anomalies propagate slightly faster, and exhibit a more pronounced propagation at larger radii compared to the inner core (Figure 4b). Individual DP events north of 30°N generally have shorter duration, smaller propagation distance, and weaker amplitude (Figures 2c, 2d and 2f). Additionally, these DPs tend to initiate later and display more variable propagation speeds (Figures 2a and 2e), suggesting that factors other than inertial-gravity waves influence DP behavior at higher latitudes.

To confirm the presence of inertial-gravity waves associated with DPs within 0°–30°N, we further examine the wave polarization relationship. The wet equivalent potential temperature θ_E (K) is calculated as derived in Rossby (1932):

$$\theta_E = T\left(\frac{1000}{P}\right)^{\frac{R}{c_p}} e^{\frac{Lq}{c_p T}}, \tag{3}$$

where L is the heat of condensation, q is the specific humidity, T is the temperature, and P is pressure. The spatial average within an 800-km radius is subtracted to remove the diurnal shortwave heating influence. Figure 4c illustrates the phase relationship between potential temperature and vertical velocity at 175 hPa. Both warming and upward anomalies display diurnal outward propagation at approximately 10 m s^{-1}, consistent with DP behavior. The observed 90° phase lag between temperature and vertical velocity aligns with the expected polarization relationship of inertial-gravity waves (Nappo, 2012).

To diagnose vertical wave propagation, we analyze the vertical cross-section of horizontal divergence anomalies in the TC outer region. Figure 4d shows opposing vertical propagation directions below and above an altitude of 14 km, with wave phases propagating upward in the troposphere and downward in the stratosphere. According to the linear gravity wave theory (Nappo, 2012), this pattern indicates that the group velocity, representing wave energy, propagates downward in the troposphere and upward in the stratosphere, originating from a wave source at the tropopause.

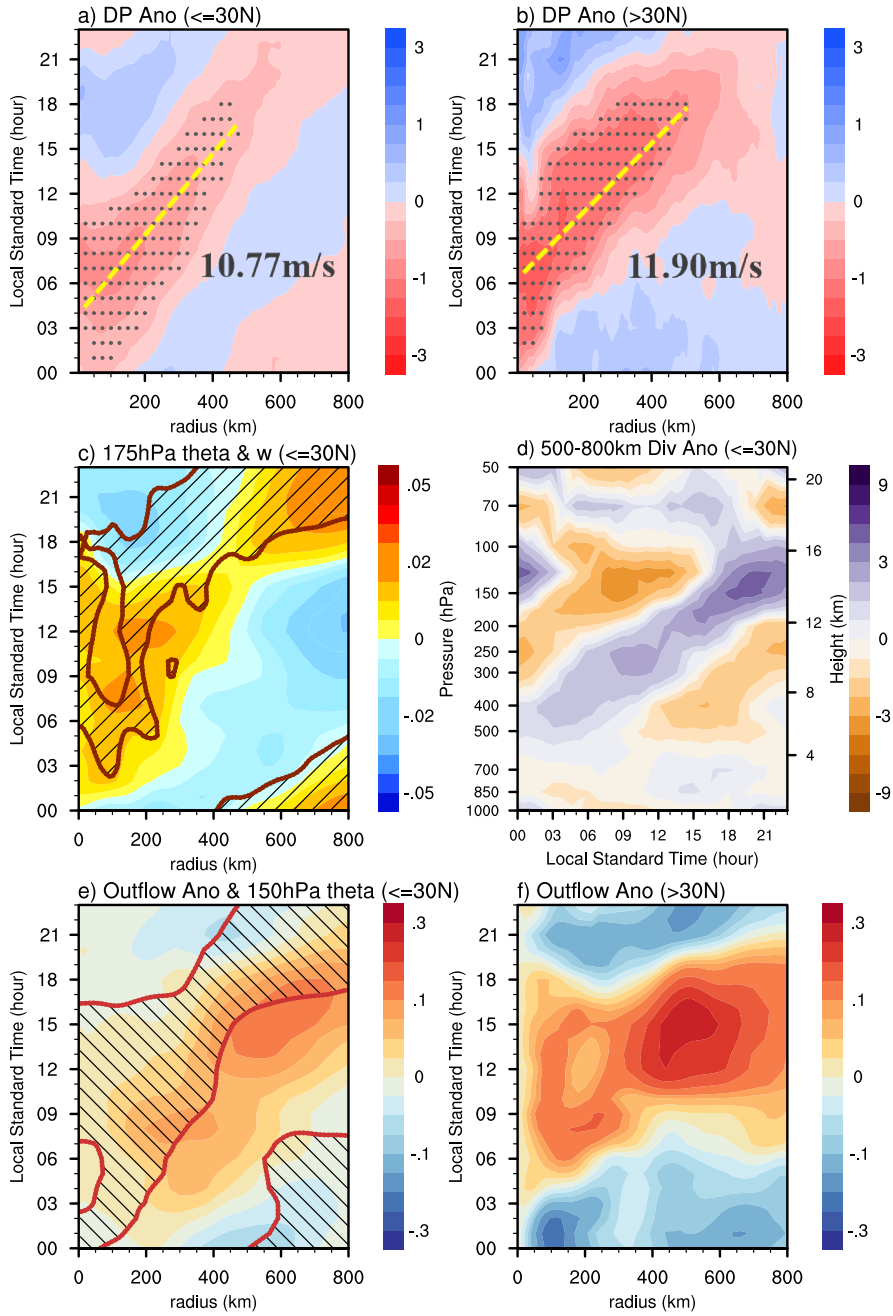

Figure 4. The composite azimuthally averaged daily anomaly characteristics. Diurnal pulse anomalies (K) (a) within 0°–30°N and (b) north of 30°N. Dots indicate grids for speed calculation. (c) Anomalies in potential temperature (shaded, K) and vertical upward motion (hatched, values less than -2×10^{-4} Pa s^{-1}) within 0°–30°N at 175 hPa. (d) Vertical section of 500–800 km radius-averaged horizontal divergence anomalies (10^{-9} s^{-1}) within 0°–30°N. TC outflow anomalies (radial wind anomalies at 150 hPa, m s^{-1}) (e) within 0°–30°N and (f) north of 30°N, with hatched area indicating warming anomalies at 150 hPa.

We hypothesize that DPs occurring north of 30°N are driven by upper-level TC outflow through wind advection effects. The statistical relationship between DP speed and outflow speed (quantified as the radial wind at 150 hPa averaged over the 200–800 km radius) further highlights the latitude dependence of DPs. For TCs north of 30°N, DP speed exhibits a positive correlation with outflow speed, with statistical significance exceeding the 95% level in the Student's *t*-test (Figure 5a2). This suggests that the afternoon-enhanced outflow, which peaks in strength

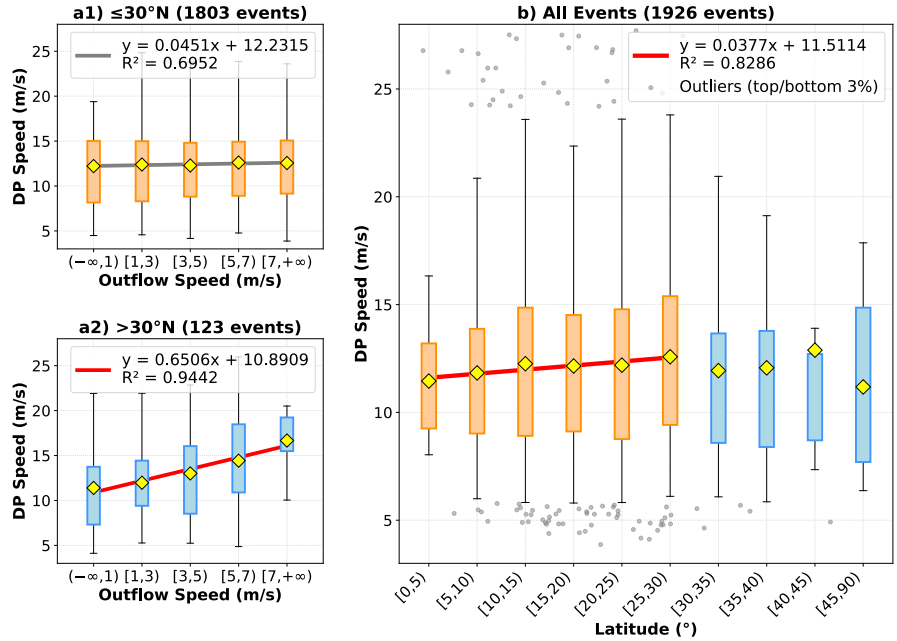

Figure 5. Box plots of diurnal pulse (DP) speeds and corresponding tropical cyclone outflow winds: (a1) within 0°–30°N and (a2) north of 30°N. (b) Box plot of DP speeds and their corresponding initial latitudes, with top and bottom 3% of outliers (dots) removed. Yellow diamonds represent the mean values, and solid lines represent linear regression, with red lines indicating statistical significance at the 0.05 level.

between 300 and 600 km radius (figure not shown), is likely responsible for the propagating signal observed in the composite DP anomalies at higher latitudes (Figure 4b). Conversely, within 0°–30°N, DP speed does not significantly correlate with outflow strength (Figure 5a1). This indicates that while DP initiation at all latitudes may be linked to common drivers such as convection or radiative processes, the mechanisms governing propagation may differ. Specifically, the propagation of DPs north of 30°N is likely influenced by the advection of TC outflow, whereas the propagation of DPs within 0°–30°N are likely governed by inertial-gravity waves.

The investigation in diurnal radial wind anomalies at 150 hPa reveals distinct differences in outflow behavior within 0°–30°N and north of 30°N. North of 30°N, outflow is enhanced during daytime (Figure 4f), consistent with the strengthening of TC's upper-level secondary circulation during the day (Figure 3b). In contrast, within 0°–30°N, outflow anomalies exhibit outward propagation (Figure 4e) similar to DP signal. Specifically, intensified radial wind anomalies precede warming anomalies, aligning with the expected wave polarization relationship. Therefore, diurnal outflow signals within 0°–30°N result from inertial-gravity waves, whereas north of 30°N, they are driven by the diurnal variations in the TC secondary circulation.

4. Discussion: Comparisons Between DP and OP

Comparing the results of this study with those of Fang and Du (2022), both DPs in TCs and OP of coastal rainfalls exhibit a strong dependence on latitude. Within 0°–30° latitude, both DP and OP occur more frequently than poleward of 30° latitude, and both are similarly driven by inertial-gravity waves. According to the dispersion equation for hydrostatic inertial-gravity waves (Equation 2), the horizontal phase speed can be calculated as:

$$c = \frac{\omega}{k} = \frac{\omega}{m}\frac{N}{\sqrt{\omega^2 - f^2}}, \tag{4}$$

This equation suggests that the wave speed theoretically increases with latitude within 0°–30° due to the Coriolis effect. Consistent with this theoretical expectation and previous findings on OP (Fang & Du, 2022), the DP speeds increase in mean values with latitude but show a more dispersed distribution (Figure 5b). This dispersion might arise from the complex background conditions within the TC environment and internal vortex dynamics,

including the effects of relative vorticity on inertial stability (Evans & Nolan, 2019; Knaff et al., 2019), which contrasts with OP, where the environment is typically more stable and closer to the ideal conditions for gravity wave propagation (Coppin & Bellon, 2019; Short et al., 2019).

Poleward of 30° latitude, in absence of inertial-gravity waves, background wind advection becomes the dominant factor influencing both OP and DP propagation. Fang and Du (2022) found that OP occurrence frequency increases under offshore winds, and similarly, DP speed positively correlates with TC outflow velocity (Figure 5a2).

5. Conclusions and Discussion

The study revisits the characteristics of outward-propagating cold-cloud DPs in TCs over the WNP from 2001 to 2022. Previous studies identified a DP discontinuity, characterized by a "two-segment signal" in composites over DP days. This study aims to explore this previously unexplained feature and investigate the underlying physical mechanisms driving this phenomenon.

1. The observed DP discontinuity results from a combination of an outward-propagating mode originating from the TC center and two inherent quasi-phase-locked modes. Unlike DP composites, the propagating mode can be isolated using DP anomalies. This outward-propagating mode initiates at 04–05 LST from the inner core and propagates continuously at a speed of approximately 10 m s^{-1}, close to phase speed of gravity waves. Meanwhile, the quasi-phase-locked modes are associated with diurnal variations in the TC secondary circulation. During the night, enhanced inner-core deep convective clouds undergo radiative cooling, while during the day, the upper-level circulation strengthens to lift and cool the cirrus canopy with more condensate away from the core.
2. DPs strongly depend on latitude, highlighting the potential role of inertial-gravity waves. Within 0°–30°N, DPs exhibit higher frequency, longer propagating distance, and stronger amplitude, likely driven by inertial-gravity waves. The wave source is located at the tropopause, where outward-propagating signals simultaneously propagate both upward or downward. North of 30°N, DPs occur less frequently, and their propagation speeds are closely linked to TC outflow strength due to background wind advection.
3. DPs in TCs and OP of coastal rainfall share similar mechanisms, both are associated with inertial-gravity waves within 0°–30° latitude, though originating from different wave sources. Poleward of 30°, both phenomena are primarily influenced by advective winds.

This study suggests that DPs are associated with inertial-gravity waves through a statistical approach, which differs from previous studies that used numerical models (Dunion et al., 2019; Navarro & Hakim, 2016; O'Neill et al., 2017; Ruppert & O'Neill, 2019). However, it remains unclear whether these waves are primarily excited by diurnal variations in radiation or convection (Dunion et al., 2014; O'Neill et al., 2017). Additionally, the impact of vertical shear direction on TC inertial-gravity waves and DPs is still not fully understood.

Moreover, while our results reveal a quasi-phase-locked cooling signal associated with the overall cloud top lifting in the afternoon on non-DP days, the all-days composite Hovmöller diagram from simulations (Figure 3a in Ruppert and O'Neill (2019)) suggest that the greater cloud top heights at larger radii propagate outward diurnally, at speeds consistent with typical DPs. This difference may arise because the all-days composite includes contributions from DP events, which exhibit outward-propagating signals not present on non-DP days.

Additionally, we find both propagating and quasi-phase-locked modes exhibit distinct characteristics across varying TC intensities and sizes, particularly in terms of propagating speed, spatial extent, and signal amplitude (Text S1 and S2, Figures S1 and S2 in Supporting Information S1). These variations may provide valuable insights into the mechanisms behind DPs, and their underlying causes require further investigation.

Future research could expand this analysis to other ocean basins to evaluate the generality of our conclusions. Additionally, further studies will explore the impacts of convection and radiation on TC diurnal gravity waves, as well as the asymmetric effects of vertical wind shear, to further advance our understanding of the DP mechanism and diurnal changes in TCs.

Conflict of Interest

The authors declare no conflicts of interest relevant to this study.

Data Availability Statement

The IBTrACS data can be accessed from National Centers for Environmental Information (NCEI) via https://www.ncei.noaa.gov/products/international-best-track-archive (Kenneth et al., 2019; Knapp et al., 2010). The GridSat-B1 data can be downloaded from NCEI via https://www.ncei.noaa.gov/products/gridded-geostationary-brightness-temperature (Knapp et al., 2011). The ERA5 data sets are available at Climate Data Store via https://cds.climate.copernicus.eu/datasets/reanalysis-era5-pressure-levels?tab=overview (Copernicus Climate Change Service, 2018).

Acknowledgments
This study was supported by the Guangdong Project of Basic and Applied Basic Research (Grants 2020B0301030004, 2024A1515510005, and 2025A1515011974), the National Natural Science Foundation of China (Grant 42475002), project supported by Southern Marine Science and Engineering Guangdong Laboratory (Zhuhai) (SML2024SP035, SML2024SP012, and 311024001), and the Key Innovation Team of the China Meteorological Administration (CMA2023ZD08). We also acknowledge the high-performance computing support from School of Atmospheric Sciences of Sun Yat-sen University.

References

Bowman, K. P., & Fowler, M. D. (2015). The diurnal cycle of precipitation in tropical cyclones. *Journal of Climate*, *28*(13), 5325–5334. https://doi.org/10.1175/JCLI-D-14-00804.1

Chen, Z., & Du, Y. (2024). The influence of topography on the diurnal rainfall propagation in the Bay of Bengal. *Journal of the Atmospheric Sciences*, *81*(6), 1019–1032. https://doi.org/10.1175/JAS-D-23-0225.1

Chen, Z., Du, Y., Vincent, C., Short, E., & Yang, H. (2025). Influence of coastal topography on offshore diurnal rainfall propagation dynamics: A linear gravity wave model approach. *Journal of the Atmospheric Sciences*. https://doi.org/10.1175/JAS-D-24-0214.1

Copernicus Climate Change Service. (2018). ERA5 hourly data on pressure levels from 1940 to present [Dataset]. *Copernicus Climate Change Service (C3S) Climate Data Store (CDS)*. https://doi.org/10.24381/CDS.BD0915C6

Coppin, D., & Bellon, G. (2019). Physical mechanisms controlling the offshore propagation of convection in the tropics: 1. Flat island. *Journal of Advances in Modeling Earth Systems*, *11*(9), 3042–3056. https://doi.org/10.1029/2019MS001793

Ditchek, S. D., Corbosiero, K. L., Fovell, R. G., & Molinari, J. (2019). Electrically active tropical cyclone diurnal pulses in the Atlantic basin. *Monthly Weather Review*, *147*(10), 3595–3607. https://doi.org/10.1175/MWR-D-19-0129.1

Ditchek, S. D., Corbosiero, K. L., Fovell, R. G., & Molinari, J. (2020). Electrically active diurnal pulses in Hurricane Harvey (2017). *Monthly Weather Review*, *148*(6), 2283–2305. https://doi.org/10.1175/MWR-D-20-0022.1

Ditchek, S. D., Molinari, J., Corbosiero, K. L., & Fovell, R. G. (2019). An objective climatology of tropical cyclone diurnal pulses in the Atlantic basin. *Monthly Weather Review*, *147*(2), 591–605. https://doi.org/10.1175/MWR-D-18-0368.1

Du, Y. (2023). Offshore migration of summer monsoon low-level jet on a diurnal scale. *Geophysical Research Letters*, *50*(20), e2023GL103840. https://doi.org/10.1029/2023GL103840

Du, Y., & Rotunno, R. (2015). Thermally driven diurnally periodic wind signals off the east coast of China. *Journal of the Atmospheric Sciences*, *72*(7), 2806–2821. https://doi.org/10.1175/JAS-D-14-0339.1

Du, Y., & Rotunno, R. (2018). Diurnal cycle of rainfall and winds near the south coast of China. *Journal of the Atmospheric Sciences*, *75*(6), 2065–2082. https://doi.org/10.1175/JAS-D-17-0397.1

Dudhia, J. (1989). Numerical study of convection observed during the winter monsoon experiment using a mesoscale two-dimensional model. *Journal of the Atmospheric Sciences*, *46*(20), 3077–3107. https://doi.org/10.1175/1520-0469(1989)046<3077:NSOCOD>2.0.CO;2

Dunion, J. P., Thorncroft, C. D., & Nolan, D. S. (2019). Tropical cyclone diurnal cycle signals in a hurricane nature run. *Monthly Weather Review*, *147*(1), 363–388. https://doi.org/10.1175/MWR-D-18-0130.1

Dunion, J. P., Thorncroft, C. D., & Velden, C. S. (2014). The tropical cyclone diurnal cycle of mature hurricanes. *Monthly Weather Review*, *142*(10), 3900–3919. https://doi.org/10.1175/MWR-D-13-00191.1

Evans, R. C., & Nolan, D. S. (2019). Balanced and radiating wave responses to diurnal heating in tropical cyclone–like vortices using a linear nonhydrostatic model. *Journal of the Atmospheric Sciences*, *76*(8), 2575–2597. https://doi.org/10.1175/JAS-D-18-0361.1

Fang, J., & Du, Y. (2022). A global survey of diurnal offshore propagation of rainfall. *Nature Communications*, *13*(1), 7437. https://doi.org/10.1038/s41467-022-34842-0

Gray, W. M., & Jacobson, R. W. (1977). Diurnal variation of deep cumulus convection. *Monthly Weather Review*, *105*(9), 1171–1188. https://doi.org/10.1175/1520-0493(1977)105<1171:DVODCC>2.0.CO;2

Hong, J., & Wu, Q. (2023). Diurnal variations of tropical cyclone outer region size growth. *Atmospheric Science Letters*, *24*(12), e1183. https://doi.org/10.1002/asl.1183

Jiang, Q. (2012). On offshore propagating diurnal waves. *Journal of the Atmospheric Sciences*, *69*(5), 1562–1581. https://doi.org/10.1175/JAS-D-11-0220.1

Kenneth, R., Howard, J., James, P., Michael, C., & Carl, J. (2019). International Best Track Archive for Climate Stewardship (IBTrACS) Project, Version 4 [Dataset]. *NOAA National Centers for Environmental Information*. https://doi.org/10.25921/82TY-9E16

Kilpatrick, T., Xie, S., & Nasuno, T. (2017). Diurnal convection-wind coupling in the Bay of Bengal. *Journal of Geophysical Research: Atmospheres*, *122*(18), 9705–9720. https://doi.org/10.1002/2017JD027271

Knaff, J. A., Slocum, C. J., & Musgrave, K. D. (2019). Quantification and exploration of diurnal oscillations in tropical cyclones. *Monthly Weather Review*, *147*(6), 2105–2121. https://doi.org/10.1175/MWR-D-18-0379.1

Knapp, K. R., Ansari, S., Bain, C. L., Bourassa, M. A., Dickinson, M. J., Funk, C., et al. (2011). Globally gridded satellite observations for climate studies. *Bulletin of the American Meteorological Society*, *92*(7), 893–907. https://doi.org/10.1175/2011BAMS3039.1

Knapp, K. R., Kruk, M. C., Levinson, D. H., Diamond, H. J., & Neumann, C. J. (2010). The International Best Track Archive for Climate Stewardship (IBTrACS): Unifying Tropical Cyclone Data. *Bulletin of the American Meteorological Society*, *91*(3), 363–376. https://doi.org/10.1175/2009BAMS2755.1

Kraus, E. B. (1963). The diurnal precipitation change over the sea. *Journal of the Atmospheric Sciences*, *20*(6), 551–556. https://doi.org/10.1175/1520-0469(1963)020<0551:TDPCOT>2.0.CO;2

Leppert, K. D., & Cecil, D. J. (2016). Tropical cyclone diurnal cycle as observed by TRMM. *Monthly Weather Review*, *144*(8), 2793–2808. https://doi.org/10.1175/MWR-D-15-0358.1

Li, Y., & Carbone, R. E. (2015). Offshore propagation of coastal precipitation. *Journal of the Atmospheric Sciences*, *72*(12), 4553–4568. https://doi.org/10.1175/JAS-D-15-0104.1

Nappo, C. J. (2012). The linear theory. In *International Geophysics* (Vol. 102, pp. 29–56). Elsevier. https://doi.org/10.1016/B978-0-12-385223-6.00002-1

Navarro, E. L., & Hakim, G. J. (2016). Idealized numerical modeling of the diurnal cycle of tropical cyclones. *Journal of the Atmospheric Sciences*, *73*(10), 4189–4201. https://doi.org/10.1175/JAS-D-15-0349.1

Navarro, E. L., Hakim, G. J., & Willoughby, H. E. (2017). Balanced response of an axisymmetric tropical cyclone to periodic diurnal heating. *Journal of the Atmospheric Sciences*, *74*(10), 3325–3337. https://doi.org/10.1175/JAS-D-16-0279.1

O'Neill, M. E., Perez-Betancourt, D., & Wing, A. A. (2017). Accessible environments for diurnal-period waves in simulated tropical cyclones. *Journal of the Atmospheric Sciences*, *74*(8), 2489–2502. https://doi.org/10.1175/JAS-D-16-0294.1

Piersante, J. O., Corbosiero, K. L., & Fovell, R. G. (2023). Simulated diurnal pulses in Hurricane Dorian (2019). *Monthly Weather Review*, *151*(11), 2869–2882. https://doi.org/10.1175/MWR-D-23-0049.1

Randall, D. A., Harshvardhan, & Dazlich, D. A. (1991). Diurnal variability of the hydrologic cycle in a general circulation model. *Journal of the Atmospheric Sciences*, *48*(1), 40–62. https://doi.org/10.1175/1520-0469(1991)048<0040:DVOTHC>2.0.CO;2

Rossby, C.-G. (1932). *Thermodynamics applied to air mass analysis*. Massachusetts Institute of Technology. https://doi.org/10.1575/1912/1139

Rotunno, R. (1983). On the linear theory of the land and sea breeze. *Journal of the Atmospheric Sciences*, *40*(8), 1999–2009. https://doi.org/10.1175/1520-0469(1983)040<1999:OTLTOT>2.0.CO;2

Ruppert, J. H., & Hohenegger, C. (2018). Diurnal circulation adjustment and organized deep convection. *Journal of Climate*, *31*(12), 4899–4916. https://doi.org/10.1175/JCLI-D-17-0693.1

Ruppert, J. H., & Johnson, R. H. (2016). On the cumulus diurnal cycle over the tropical warm pool. *Journal of Advances in Modeling Earth Systems*, *8*(2), 669–690. https://doi.org/10.1002/2015MS000610

Ruppert, J. H., & O'Neill, M. E. (2019). Diurnal cloud and circulation changes in simulated tropical cyclones. *Geophysical Research Letters*, *46*(1), 502–511. https://doi.org/10.1029/2018GL081302

Short, E., Vincent, C. L., & Lane, T. P. (2019). Diurnal cycle of surface winds in the maritime continent observed through satellite scatterometry. *Monthly Weather Review*, *147*(6), 2023–2044. https://doi.org/10.1175/MWR-D-18-0433.1

Tang, X., & Zhang, F. (2016). Impacts of the diurnal radiation cycle on the formation, intensity, and structure of Hurricane Edouard (2014). *Journal of the Atmospheric Sciences*, *73*(7), 2871–2892. https://doi.org/10.1175/JAS-D-15-0283.1

Tao, W.-K., Lang, S., Simpson, J., Sui, C.-H., Ferrier, B., & Chou, M.-D. (1996). Mechanisms of cloud-radiation interaction in the tropics and midlatitudes. *Journal of the Atmospheric Sciences*, *53*(18), 2624–2651. https://doi.org/10.1175/1520-0469(1996)053<2624:MOCRII>2.0.CO;2

Trabing, B. C., & Bell, M. M. (2021). Observations of diurnal variability under the cirrus canopy of Typhoon Kong-rey (2018). *Monthly Weather Review*. https://doi.org/10.1175/MWR-D-20-0327.1

Wu, Q., & Ruan, Z. (2016). Diurnal variations of the areas and temperatures in tropical cyclone clouds. *Quarterly Journal of the Royal Meteorological Society*, *142*(700), 2788–2796. https://doi.org/10.1002/qj.2868

Wu, Q., Ruan, Z., Chen, D., & Lian, T. (2015). Diurnal variations of tropical cyclone precipitation in the inner and outer rainbands. *Journal of Geophysical Research: Atmospheres*, *120*(1), 1–11. https://doi.org/10.1002/2014JD022190

Zhang, J. A., Dunion, J. P., & Nolan, D. S. (2020). In situ observations of the diurnal variation in the boundary layer of mature hurricanes. *Geophysical Research Letters*, *47*(3), 2019GL086206. https://doi.org/10.1029/2019GL086206

Zhang, X., Ditchek, S. D., Corbosiero, K. L., & Xu, W. (2023). Global and regional characteristics of radially outward propagating tropical cyclone diurnal pulses. *Journal of Geophysical Research: Atmospheres*, *128*(7), e2022JD037660. https://doi.org/10.1029/2022JD037660

Zhang, X., & Xu, W. (2021). Strong diurnal pulsing of cold clouds in rapidly intensifying tropical cyclones. *Geophysical Research Letters*, *48*(21), e2021GL094773. https://doi.org/10.1029/2021GL094773

Zhang, X., & Xu, W. (2022). Is there an outward propagating diurnal signal in the precipitation of tropical cyclones? *Geophysical Research Letters*, *49*(4). https://doi.org/10.1029/2021GL097166

Zhang, X., & Xu, W. (2024). Changes in the deep convective structures of tropical cyclones associated with the diurnal pulse. *Journal of Geophysical Research: Atmospheres*, *129*(24), e2024JD041441. https://doi.org/10.1029/2024JD041441